Available online at www.sciencedirect.com
SCIENCE DIRECT®
Journal of Power Sources 126 (2004) 76–87
JOURNAL OF POWER SOURCES
www.elsevier.com/locate/jpowsour

A numerical study of cell-to-cell variations in a SOFC stack

A.C. Burt [a], I.B. Celik [a,*], R.S. Gemmen [b], A.V. Smirnov [a]

[a] *Mechanical and Aerospace Engineering Department, West Virginia University, Morgantown, WV 26506, USA*
[b] *US DOE National Energy Technology Laboratory, Morgantown, WV 26507, USA*

Received 29 July 2003; accepted 25 August 2003

Abstract

A numerical investigation of cell-to-cell voltage variation is performed by considering the impact of flow distribution and heat transfer on a SOFC stack. The stack model used is based on a one-dimensional co-flow cell model developed in prior work. The influence of radiative heat transfer between the PEN (positive electrode, electrolyte, negative electrode body) and the neighboring separator plates on the temperature distribution is also considered. Variations in cell voltage are attributed to asymmetries in stack geometry (boundary effects) and non-uniformity in flow rates, more particularly, flow thermal capacity. Simulations were done in a parallel computing environment with each cell computed in a separate (CPU) process. This natural decomposition of the fuel cell stack reduced the number of communicated variables thereby improving computational performance. The parallelization scheme implemented utilized a message passing interface (MPI) protocol where cell-to-cell communication is achieved via exchange of temperature and thermal fluxes between neighboring cells.

Keywords: Fuel cell modeling; Solid oxide fuel cell; Stack modeling; Variation in cell-to-cell performance

1. Introduction

In recent years emphasis has been placed on the development of affordable clean power sources. This has caused much speculation about the use of fuel cell technology in various endeavors; e.g., automobiles, stationary power generation, portable power supplies, etc. There are many fuel cell types, with the most common ones being: phosphoric-acid fuel cells (PAFC), solid-oxide fuel cells (SOFC), molten-carbonate fuel cells (MCFC), alkaline fuel cells (AFC), proton exchange membrane (PEM), and direct methanol fuel cells (DMFC) [1]. Regardless of the type of cell, stacks of cells (in electric-series) can be used to generate desired voltage output and power. The SOFC shows a high potential for being an efficient and clean solution for stationary based power generation.

At the heart of a solid oxide fuel cell is the solid electrolyte (usually made of stabilized zirconia) which at temperatures >600 °C conducts oxygen ions from the porous cathode to the porous anode [2]. At the cathode triple interface where the electrically conducting electrode, ionically conducting electrolyte, and cathode gas phase meet, oxygen is electrochemically reduced (ionized) and enters the electrolyte to be transported across to the anode. At the anode triple interface where the anode electrode, electrolyte, and anode gas channel meet, the oxygen ions react with hydrogen and carbon monoxide to form water and carbon dioxide, respectively. The electrons released in the charge transfer reaction of oxygen enter the anode electrode and can then pass through an external load on their way back to the cathode and in the process release useful energy. The cathode electrode, electrolyte, and anode electrode together are called PEN. In general, the gas flow through the anode and cathode gas channels results in forced convective heat transfer, and presently it is common to see units operating at pressures close to atmospheric. In an ideal situation it is desirable to have all of the cells in a stack to perform uniformly. It has been observed experimentally that usually the cells in a stack do not operate uniformly [3,4]. The cause of the variations is not well understood. Significant variations among the cells may cause long run structural problems and may eventually lead to total failure of the power generation unit. Possible causes are non-uniform fuel/air flow distribution to individual cells, non-uniform temperature and/or current distribution within the stack [5], and material non-uniformities. At the desired high utilization rates of fuel (>70%) such flow non-uniformity can be limiting. However, all of these factors are interrelated hence a systematic investigation is necessary to better understand the root causes. Previous studies by Hirata and Hori [6], Costamagna and Honegger [7], Achenbach

* Corresponding author. Tel.: +1-304-293-3111; fax: +1-304-293-6689.
E-mail addresses: ismail.celik@wvu.edu (I.B. Celik), randall.gemmen@netl.doe.gov (R.S. Gemmen).

0378-7753/$ – see front matter © 2003 Elsevier B.V. All rights reserved.
doi:10.1016/j.jpowsour.2003.08.034

Nomenclature

A_1	area of surface (m^2)
A_{XS}	cross-sectional area (m^2)
e	energy per unit mass (J/kg)
E	open circuit potential (V)
E^0	potential at standard state conditions (V)
E_{cor}	corrected potential (V)
F	Faraday constant (C/mol)
F_{12}	shape factor from surface 1 to 2 (1)
F_x	forces in x- (streamwise-)direction (N)
G	Gibbs free energy (kJ/kg)
ΔH_{H_2O}	heat of formation for H_2O (kJ/kg mol)
h_c	convective heat transfer coefficient (W/m^2 K)
i_0	exchange current (A/m^2)
i_{den}	current density (A/m^2)
k	thermal conductivity (W/m K)
l_w	width of control volume (1 m)
L	cell length (m)
$\dot{m}''$	mass flux per area (kg/m^2 s)
$\dot{m}_{surf}$	net mass flux through surface (kg/s)
n	number of participating electrons
Nu	Nusselt number (1)
P	pressure (Pa)
P^0	reference pressure (Pa)
Pr	Prandtl number (1)
$\dot{Q}_{conv}$	convective heat transfer rate (W)
$\dot{Q}_{gen}$	rate of heat generation (W)
$\dot{Q}_{net}$	net heat transfer rate (W)
$\dot{Q}_{rad}$	radiative heat transfer rate (W)
R	resistance ($\Omega\,m^2$)
Re	Reynolds number (1)
R_{net}	net resistance ($\Omega\,m^2$)
R_u	universal gas constant
s	entropy per mole (kJ/(kmol K)
t	time (s)
T	temperature (K)
T_{surf}	surface temperature (K)
T_{env}	temperature of the environment (K)
u	velocity in x-direction (m/s)
Δx	length of control volume in x-direction (m)
X_k	mole fraction (1)
Y_k	mass fraction (1)

Greek letters

α	transfer coefficient (1)
ε	total emittance (1)
η_{act}	activation loss (V)
η_{conc}	concentration loss (V)
η_{Ohm}	Ohmic loss (V)
ρ	mixture density (kg/m^3)
σ	Stefan–Boltzmann constant (W/m^2 K)
$\dot{\omega}_k$	rate of formation and destruction of specie (K)
$\forall$	volume (m^3)

Subscripts and Superscripts

1	surface 1
2	surface 2
k	*k*th specie
e	east face of control volume
env	environment
H_2	hydrogen gas
H_2O	water vapor
n	north face of control volume
O_2	oxygen gas
s	south face of control volume
surf	surface of control volume
w	west face of control volume
xs	cross-sectional area

Abbreviations

1D	one dimensional
2D	two dimensional
3D	three dimensional
MCFC	molten carbonate fuel cell
PEN	positive electrode, electrolyte, and negative electrode
SOFC	solid oxide fuel cell

[8], and Ma [9] attempted to elucidate some of the factors but some questions such as the influence of non-symmetry and non-uniform flow distribution are left unanswered. In this study, we investigate the influence of variations in inlet flow rates on the performance of individual cells connected in series within a stack.

During the course of the earlier stages of this study, it was found that there were significant temperature differences within the stack as a result of natural non-symmetry that exists in a stack arranged by simply connecting cells in series. These observations lead to the investigation of the role of radiative heat transfer on the eventual temperature distribution within the stack. Solid oxide fuel cells usually operate at high temperatures in the range (700–1200 °C) utilizing a variety of fuels (i.e. hydrogen gas, hydrocarbons, and carbon monoxide) [2,10,11]. At these elevated temperatures thermal radiation emitted from the solid elements of the fuel cell may constitute a noticeable portion of the heat transfer within the stack.

In the literature, there are numerous studies [6–9,12,13] which are similar in concept to the present one but have not included some unique features. For example the treatment of radiation heat transfer was often neglected. Aguiar et al. [12] developed a 2D model for the internal indirect reformer, and coupled it with a 1D model for the SOFC. The

SOFC model combined the porous anode and cathode electrodes with the electrolyte as a single solid structure (PEN). A similar modeling approach was used in the present study. Aguiar et al. [12] included radiation between the PEN and reformer using assumption of two long concentric cylinders. An emissivity of 0.9 was used for both surfaces of the solid structure and the reformer. Their results show that radiative heat transfer accounted for up to 79% of the total heat transfer between the solid structure and the reformer. Hirata and Hori [6] consider radiative heat transfer between the PEN and the separator plate in a manner similar to the present study but for a MCFC stack. In their study, an emissivity of 0.48 and a view factor of 1 was used. The gas was considered to be non-participating. Costamagna and Honegger [7] considered a planar cylindrical SOFC operating in a co-flow configuration. In their model, they consider the stack to have insulated top and bottom plates this is the same as in the present study. In both Costamagna and Honeggar [7] and Achenbach [8], radiation was considered between the stack and the surrounding shell as part of the boundary condition for the stack but the radiation between individual PEN and separator plate was neglected. Yakabe et al. [13] considered a single SOFC cell in a counter-flow configuration using a 3D model. However, no radiation model was used because the temperature was considered to be uniform everywhere in the cell. Virkar et al. [14], like Yakabe et al. [13], also used a uniform temperature in their study which focused on comparison of electrolyte versus electrode supported cell and the impact of composite electrodes. Ma [9] neglected radiation heat transfer effects because channels were considered to be thin and the cells were considered to be at nearly the same temperature. The above brief literature review show that the importance and the effects of radiation heat transfer have yet to be fully realized.

In order to increase fuel cell performance and reliability and reduce costs suitable designs must be developed. Effective computational models provide insight into design performance and allow developers the tools needed to start with a good design. Accuracy of predictions, resolution of design details, and execution speed of computer simulations are important considerations when developing numerical models. Generally one is traded off for the other in an attempt to find a cost effective solution. Detailed analysis of a SOFC stack using computational fluid dynamics (CFD) modeling requires immense resources and computational time and quickly becomes unaffordable for the modeling of large stacks (100 cells or more). A less detailed cell based pseudo-one dimensional (POD) model provides a means for the study of large stacks by reducing the problem to essentially a 1D analysis based on changes in the streamwise direction. An efficient and robust 1D model of a fuel cell stack allows for quick parametric studies and hence is cost effective in design analysis. This is the approach used in the present study.

The primary objective of the current work is to provide a framework based on fairly simple mathematical and computational models to understand possible reasons for cell-to-cell performance variations, and the physical factors that may mitigate these variations, so that new strategies can be planned to achieve uniformity among individual cells. A 1D single cell model was extended to the case of a stack of cells using domain decomposition for parallel execution of the code. The parallelization strategy is also presented in this paper.

2. Computational model

The fuel-cell stack has been divided into computational domains using domain decomposition with each cell being treated as a separate process (see Fig. 1a) on a distributed memory multi-processor system, such as a Beowulf cluster. Communication between domains or processes was accomplished using the Message Passing Interface (MPI) library.

Each cell was further divided into control volumes. Fig. 1b depicts the control volume approximation used for mass conservation and is similarly defined for the other

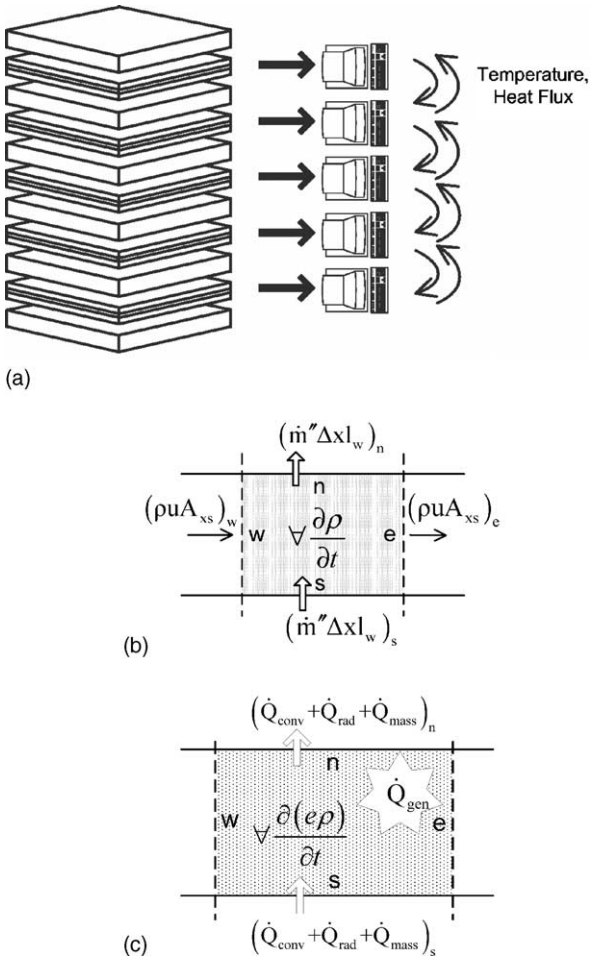

Fig. 1. (a) Domain decomposition for a five cell stack, where each cell is treated as an individual process on a separate computer processor. (b) Gas channel control volume for mass conservation. (c) Electrolyte control volume for energy conservation.

conservation equations. A one dimensional model was implemented where the variations in the streamwise (x-)direction are explicitly calculated, those in the vertical (y-)direction are accounted for via integral approximations, and those in the transverse (z-)direction are neglected. This analysis was applied to the fuel cell anode gas channel, electrolyte plate, cathode gas channel, and separator plate. Each control volume of the fuel and air gas channels was required to satisfy the following governing equations for mass, momentum, and energy, respectively:

$$\forall\frac{\partial\rho}{\partial t} + (\rho u A_{xs})_w - (\rho u A_{xs})_e = \dot{m}_{surf} \tag{1}$$

$$\forall\frac{\partial(u\rho)}{\partial t} + (u\rho u A_{xs})_w - (u\rho u A_{xs})_e = \sum F_x \tag{2}$$

$$\forall\frac{\partial(e\rho)}{\partial t} + (e\rho u A_{xs})_w - (e\rho u A_{xs})_e = \dot{Q}_{conv} \tag{3}$$

where

$$\dot{m}_{surf} = (\dot{m}''\Delta x l_w)_s - (\dot{m}''\Delta x l_w)_n$$

and the symbols are explained in nomenclature. Specie mass conservation was satisfied using

$$\frac{\forall\partial(\rho Y_k)}{\partial t} + (\rho Y_k u A_{xs})_w - (\rho Y_k u A_{xs})_e = \dot{\omega}_k \Delta x l_w \tag{4}$$

In Eqs. (1)-(4), it is assumed that changes in the x-direction are small, therefore, diffusion terms are neglected, i.e. the usual thin boundary layer assumption is invoked. The energy Eq. (3) is used to determine the temperature, and the current density is determined by an electrochemical model (Gemmen et al. [17]) using a simplified Butler–Volmer relation. Then, the current density and temperature are used to calculate appropriate fluxes which are introduced as source (or sink) terms for each of the conservation equations. The molar flux of a given species k is obtained from the current density using:

$$\dot{\omega}_k = \frac{-i_{den}}{n_k F} \tag{5}$$

where n is the number of electrons per mole of reactant k.

The PEN and separator plate are considered to be made of solid material; therefore, only the energy equation (that essentially reduces to the heat conduction equation) was solved in these regions which was simplified from Eq. (3) to:

$$\forall\frac{\partial(e\rho)}{\partial t} = \dot{Q}_{net} + \dot{Q}_{conv} \tag{6}$$

The radiative and convective heat flux through the surface of the control volume, and the thermal energy transported by mass–flux, are all included in $\dot{Q}_{net}$ (see Eq. (16)), and the heat source, $\dot{Q}_{gen}$, is obtained from Ohmic heating and heat of entropy generation resulting in the following expression:

$$\dot{Q}_{gen} = (i_{den})^2 R + T\Delta s\dot{\omega}_{H_2} \tag{7a}$$

The total entropy change per mole, Δs is obtained from:

$$\Delta s = \Delta\bar{s}^0 + R_u \ln\frac{r_R}{r_P} \tag{7b}$$

where $\Delta\bar{s}^0$ is the molar change in entropy at standard conditions and r_R and r_P are the reactant and product activities, respectively.

Pressure, P, is calculated from the ideal gas law:

$$P = \rho R_u T \tag{8}$$

The electrochemistry model is based on the assumption that the overall chemical reaction occurring in the fuel cell is:

$$H_{2(g)} + \tfrac{1}{2}O_{2(g)} \rightarrow H_2O_{(g)} \tag{9}$$

Calculation of the cell potential starts with the Nernst equation:

$$E = E^0 + \frac{R_u T}{2F}\ln\left[\frac{[X_{H_2}][X_{O_2}]^{1/2}}{[X_{H_2O}]}\right] + \frac{R_u T}{4F}\ln\frac{P}{P^0} \tag{10}$$

The pressure is assumed to be the same for both the anode and cathode gas channels. The reversible potential at standard state conditions is obtained from the change in the standard Gibbs free energy.

$$E^0 = \frac{\Delta G^0}{nF} \tag{11}$$

The corrected cell potential, E_{cor}, is obtained by subtracting the Ohmic (η_{Ohm}), concentration (η_{conc}), and activation (η_{act}) losses (i.e. over potentials) from the ideal Nernst potential, E:

$$E_{cor} = E - \eta_{Ohm} - \eta_{conc} - \eta_{act} \tag{12}$$

The overpotentials are related to the current density. The activation over-potential is defined by an empirical relation represented by a limiting form of the Butler–Volmer equation.

$$\eta_{Ohm} = i_{den} R_{net} \tag{13}$$

$$\eta_{conc} = -\frac{R_u T}{nF}\ln\left(1 - \frac{i_{den}}{i_L}\right) \tag{14}$$

$$\eta_{act} = \frac{R_u T}{n\alpha F}\ln\left(\frac{i_{den}}{i_0}\right) \tag{15}$$

A quasi-steady gas option was used whereby the gas flow was determined from empirical steady-state relations, e.g. a steady-state friction coefficient equation. This allowed large time steps to be used with the time marching scheme to reach a steady-state solution. More details about the mathematical model can be found in previous work [15–17].

2.1. Convective and radiative heat transfer

When considering the heat flux from the PEN and separator plate it can be noted that there are two main modes of

heat transfer, convective heat transfer between the solid and gas phase (which includes the effect of bulk mass transport to/from the electrolyte surface), and radiative heat transfer between the solid and the neighboring solid surfaces. These are both included in $\dot{Q}_{net}$, the net boundary heat flux through the top and bottom surfaces of the computational volume (see Fig. 1c), in Eq. (6). Thus $\dot{Q}_{net}$ is obtained from

$$\dot{Q}_{net} = (\dot{Q}_{conv} + \dot{Q}_{rad} + \dot{Q}_{mass})_s - (\dot{Q}_{conv} + \dot{Q}_{rad} + \dot{Q}_{mass})_n \quad (16)$$

where $\dot{Q}_{mass}$ is the net heat transfer due to mass transport through the electrolyte and, therefore, is zero for the separator plate.

The convective heat transfer rate is given by

$$\dot{Q}_{conv} = h_c A_1 (T_{surf} - T_{env}) \quad (17)$$

An empirical Nusselt number correlation is used of the form

$$Nu = f(Re, Pr) \quad (18)$$

which, in turn, is used to calculate h_c from

$$Nu = \frac{h_c L}{k} \quad (19)$$

In general, the radiative heat transfer between the two surfaces 1 and 2 can be calculated from

$$\dot{Q}_{rad} = A_1 F_{12} (\varepsilon_1 \sigma T_1^4 - \varepsilon_2 \sigma T_2^4) \quad (20)$$

Initially, when considering the radiative heat transfer several simplifying assumptions were made [18]. The width of the gas channels is small (on the order of 1 mm) this would result in the product of partial pressure and path length also being small. When considering water vapor in the fuel gas channel a total emissivity of much less than 0.007 was estimated (see Figs. 17–13 in Siegel and Howell [19]). Therefore, the gas medium between the surfaces is considered to be non-participating. The PEN and separator plate are considered to have black surfaces (having an emissivity, ε=1). The view factor, F, is assumed to be 1. Therefore, all emitted radiation is considered to be absorbed by the surface of the opposite plate. With these simplifications the radiative heat transfer rate, $\dot{Q}_{rad}$, can be expressed as:

$$\dot{Q}_{rad} = A_1 \sigma (T_1^4 - T_2^4) \quad (21)$$

It is not known what the exact radiative properties are for a generic fuel cell. Therefore, in this study the results with and without radiation are compared. Eq. (21) should give a conservative estimate for the heat transfer rate due to radiation. Considering heat absorbed by a participating medium (i.e. gases in the anode and cathode channels) and modeling the surfaces of the electrodes and separator plates as grey surfaces would reduce the overall influence of the radiative heat transfer.

2.2. Numerical method

As previously noted the computational domain was divided into control volumes along the streamwise direction. A staggered grid is used where the velocity is stored at the control volume east and west face and the pressure is stored at the control volume center. The solution was obtained by solving the conservation equations (Eqs. (1)-(4), and (6)) explicitly using a finite volume approach in conjunction with backward Euler method in time. The approach marches in time using a time step determined by a limiting change in temperature for the energy equation. First the boundary conditions are updated by simultaneously calculating the quasi-steady gas phase solution and the distribution of current density over the cell. Then the minimum time step is calculated. The time step, heat flux, and surface temperatures are then communicated between neighboring cells in the stack. The transient fuel cell temperature is then analyzed by solving the top plate, anode gas channel, cathode gas channel, PEN, and separator plate equations. Analysis is conducted starting from the first control volume and proceeds in the streamwise direction.

A grid convergence analysis was performed on a 2 cell stack using 5, 8, 10, 15, and 20 nodes. Beyond 15 nodes the differences in steady-state solutions were negligible. The results presented in this paper were obtained using 20 computational cells in the x-direction.

2.3. Creation of a stack model

In the current simulation approach the modular structure of a fuel-cell stack was exploited, which enables a straightforward application of the domain decomposition technique for parallel implementation of the code. This is done by simulating each cell with a separate process in a multi-processor computing environment. Since the processes inside each fuel cell are relatively independent from other cells and are coupled only through the well defined fluxes (i.e. heat, mass, current), and the given boundary conditions (voltage, temperature, pressure, etc.), it is possible to arrange a stable and time accurate parallel iteration procedure for a coupled solution of cell properties in the stack without excessive communication overhead. In this implementation, temperature, thermal fluxes (convective and radiative), time step, and termination bit are communicated between processes using MPI to simulate the stack. This parallel solver can be run on a distributed memory computer platform, such as a Beowulf cluster.

A stack of cells can be modeled using several instances of individual cells. MPI library calls are used to communicate variable data between neighboring cells. Each cell in a stack is considered to be in series, therefore, the same total current is maintained by all cells. The smallest time step is used by all cells, because all equations for the stack of cells must be solved using the same time stepping.

As the separator plate is not porous only thermal transfer must be considered between neighboring cells. The

temperature of the separator plate of each cell is communicated to the adjoining cell. The convective and radiative heat fluxes are then calculated using the received temperature from the neighbor. These fluxes are then shared between cells and are used when calculating the temperature of the separator plate, anode gas channel, and electrolyte plate at the new time level.

Each cell process is executed independently, therefore, it is important for a break signal to be communicated to all cells. In this way, if one cell must stop execution all cells will also stop. Through careful communication it is, therefore, possible to model a stack of cells using individual processes. The limited number of variables that must be communicated makes decomposition of a fuel cell stack a prime candidate for parallel programming.

2.4. The pseudo 2D stack model

As described above, the individual components of the fuel cell are considered using 1D layers, e.g. fuel channel (layer 1), PEN (layer 2), air channel (layer 3), etc. Communication of fluxes and current density, between layers (as explained above) allows for what may be called a pseudo 2D solution to be obtained. This approach used in the single cell model is expanded to include multiple cells in a stack with temperature, heat flux, and total current communicated between neighboring cells. Thus, the model has effectively become 2D via layering and stacking. This allowed extracting 2D temperature contours (e.g., see Fig. 2a and b), albeit the numerical grid in the transverse direction (y-direction normal to the flow direction) is coarse due to the nature of the model.

3. Application

The stack model described above was applied to the case of a five cell planar SOFC stack. Fig. 3 depicts the physical geometry of a single cell (or unit cell) when visualized from the side. The fuel and oxidizer are introduced to the cell in a co-flow configuration. For illustration, in Fig. 3 the cell has been divided in the x-direction into five computational control volumes denoted by i. The active area of the cell is modeled by the computational nodes 1–3 in figure. In the actual study the cell was divided into 20 computational nodes in the streamwise direction. T_{Top} and T_{Bottom} are extra storage arrays used for communication of temperature between neighboring cells in the stack. In the case of the top and bottom cells, these arrays are also used to specify ambient temperatures useful for modeling heat transfer to the stack surroundings. In the current study, the heat flux from the fuel cell stack to the surroundings is zero, representative of a perfectly insulated wall boundary condition on the top and bottom of the stack.

The physical geometry of the stack is defined by the length of the cell in the streamwise direction, and the thickness of each component. These dimensions are listed in Table 1 for

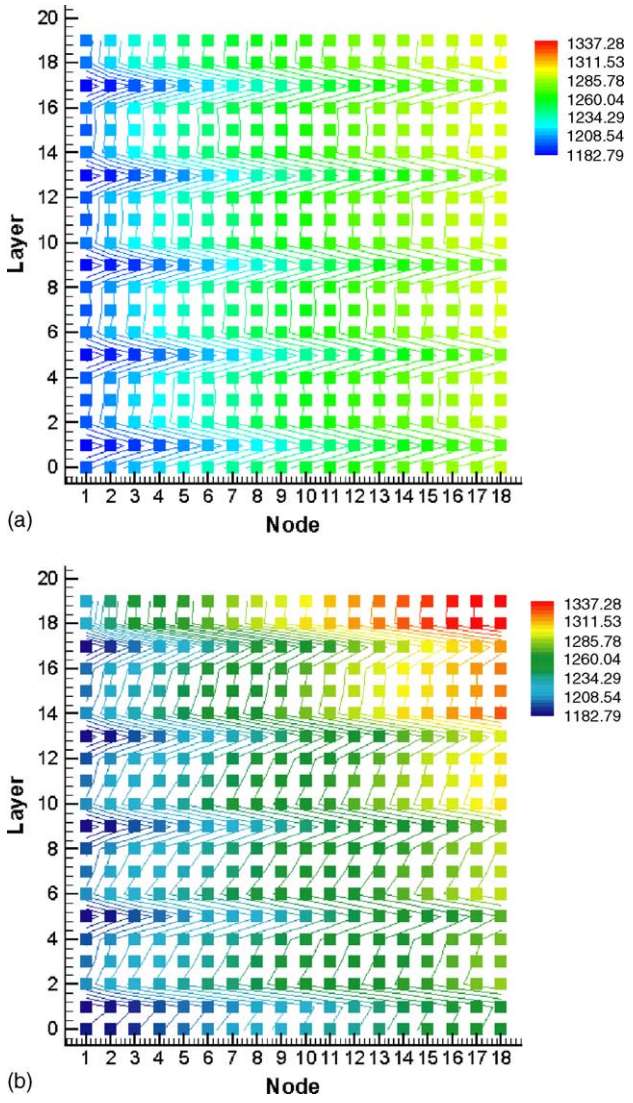

Fig. 2. Temperature contours for uniform flow case at average current density = 3333 A/m^2: (a) with radiative heat transfer; (b) neglecting radiative heat transfer.

an electrolyte supported cell. The PEN has a thickness defined by the sum of the thickness of anode electrode, electrolyte, and cathode electrode. In addition, the anode and cathode gas channel gap thicknesses must be specified. For the current study both an electrolyte and anode supported cell geometry was investigated.

Table 1
Physical dimensions of single fuel cell with electrolyte support

SOFC component	m
Cell length	1.0E − 01
Anode gas channel gap	1.0E − 03
Cathode gas channel gap	3.0E − 03
Electrolyte thickness	1.8E − 04
Anode electrode thickness	5.0E − 05
Cathode electrode thickness	5.0E − 05
Separator thickness	2.0E − 03

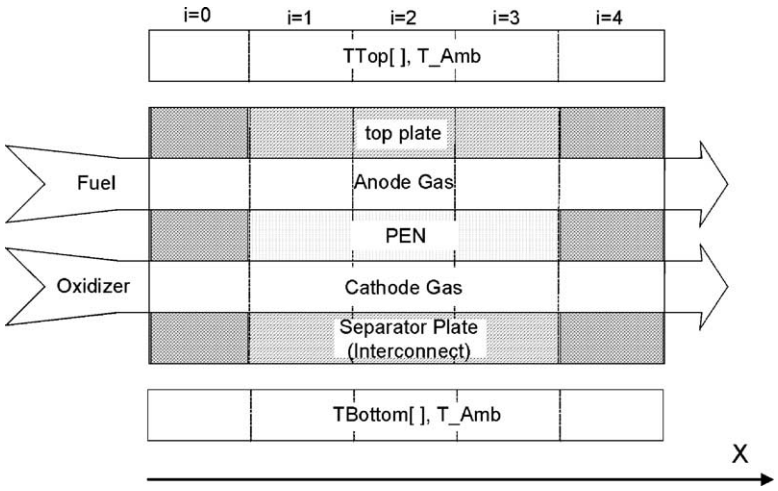

Fig. 3. Physical geometry of a single cell.

Material properties and model parameters listed in Table 2 were taken from prior work [17,20]. The stack is considered to be homogeneous with all the cells being constructed with the same physical dimensions and material properties. The inlet and outlet boundary conditions applied to the governing equations (continuity, energy conservation, species-mass conservation, and momentum equation) and electrochemistry model parameters are listed in Table 2.

Fuel utilization is of major concern and, therefore, fuel mass flow rates are generally set to insure high H_2 utilization. Numerical experiments were performed with various inlet velocities prescribed for the anode gas channel. This study consisted of six cases (Cases A–F) having the same total anode flow rate, but used different flow rates on individual cells. Table 3 presents the prescribed inlet velocities (relative input flow rates) for the anode gas channel. A numbering convention was used to identify the cells in a manner similar to levels in a building (with cell number increasing in the vertical direction). For Case A (referred to as the base case), uniform flow distribution was prescribed. Each of the other cases involved redistributing 20% of the flow in the anode gas channel of the bottom cell to the other cells in the stack.

The six cases were computed for different current demands ranging from 50–650 A. The study was conducted with electrolyte supported geometries and with high and low oxygen utilizations obtained by specifying inlet mass flow rates of 1.09×10^{-3} and 5.45×10^{-3} kg/s for the cathode gas channel. An anode supported geometry was also investigated for Cases A and C for comparison.

Table 2
Material properties and model parameters

	m
Cell heat capacity (J/kg K)	8.00E + 02
Cell density (kg/m^3)	1.50E + 03
Separator heat capacity (J/kg K)	4.00E + 02
Separator density (kg/m^3)	8.00E + 03
No. of axial nodes	20
Anode inlet temperature (K)	1.17E + 03
Anode inlet pressure (Pa)	1.01E + 05
Anode exit pressure (Pa)	1.01E + 05
H_2 anode inlet mole fraction	9.70E − 01
H_2O anode inlet mole fraction	3.00E − 02
Cathode inlet temperature (K)	1.17E + 03
Cathode inlet pressure (Pa)	1.01E + 05
Cathode exit pressure (Pa)	1.01E + 05
O_2 cathode inlet mole fraction	2.10E − 01
N_2 cathode inlet mole fraction	7.90E − 01
Contact + separator resistance (Ω/cm^2)	1.0E − 01
Limiting current density (A/m^2)	4.0E + 03
Exchange current density (A/m^2) @ 1273 K	5.5E + 03

Table 3
Prescribed anode inlet velocity (m/s) for the six test cases

	A	B	C	D	E	F
4	0.4070	0.4274	0.4070	0.4070	0.4070	0.4884
3	0.4070	0.4274	0.4070	0.4070	0.4884	0.4070
2	0.4070	0.4274	0.4070	0.4884	0.4070	0.4070
1	0.4070	0.4274	0.4884	0.4070	0.4070	0.4070
0	0.4070	0.3256	0.3256	0.3256	0.3256	0.3256
Total	2.0350	2.0350	2.0350	2.0350	2.0350	2.0350

4. Results and discussion

Performance of the SOFC stack was studied by holding the flow rate constant and allowing the utilization to vary with current load. For reference, the range of overall stack hydrogen and oxygen utilization for all cases are shown in Fig. 4. Results are presented for the electrolyte supported geometry cases. The influence of radiation heat transfer is assessed by comparing results from runs with and without

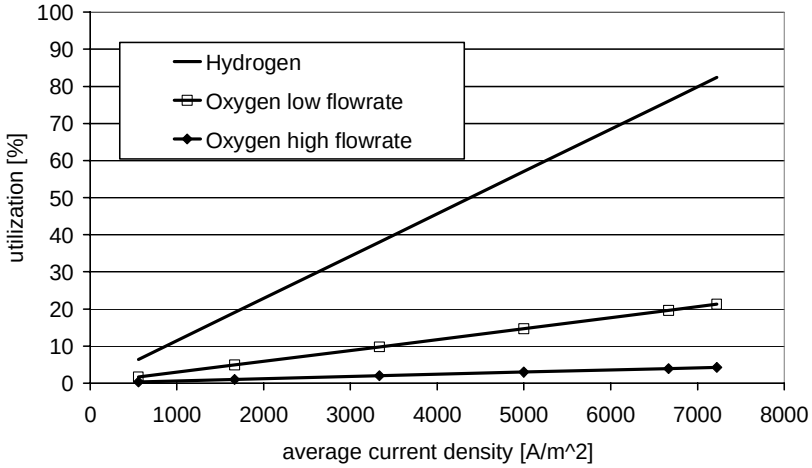

Fig. 4. Utilization at different current densities; for oxygen utilization, two curves are shown, one at high air flow rate of 5.45×10^{-3} kg/s and the other at low air flow rate of 1.09×10^{-3} kg/s.

radiation. The discussion then continues by considering several cases were non-uniform flow distributions are prescribed for the anode gas channels. Changes in cell voltage resulting from changing the air flow rate are considered. Finally, an anode supported geometry is considered.

4.1. Effect of radiation—electrolyte supported cell

Fig. 2a shows the temperature distribution through the stack for the case with radiation. For this analysis, steady-state solutions were obtained for a stack made of five electrolyte supported cells providing a total current of 300 A (average current density of 3333 A/m^2). Air was supplied to the cathode gas channel at 1.09×10^{-3} kg/s resulting in c.a. 10% oxygen utilization (see Fig. 4). Significant variations in cell temperature are observed from the top to the bottom of the stack. The fuel cell stack geometry is inherently asymmetric. The stack is operating with different cathode and anode mass flow rates causing the heat transfer coefficient and thermal capacity to vary between gas channels. The air gas channel has the highest mass flow rate (and thermal capacity) and, therefore, provides the most cooling. This asymmetry is the dominant cause for the non-uniformity seen in temperature distribution in the fuel cell stack. Hence, the top cell does not suffer from the presence of a cooling cathode gas channel that a neighboring cell would provide. Likewise, the bottom cell does not benefit from the heat that a neighboring cell would provide. The result, as shown in Fig. 2a and b, is that the top cell operates at the highest temperature and the bottom cell operates at the lowest temperature. The most notable contours are the cool cathode gas channels.

Fig. 2b shows the temperature profile through the stack for the case where radiative heat transfer is neglected. Comparing Fig. 2a and b show that the neglect of radiative heat transfer resulted in increased non-uniformity of the temperature distribution within the stack. Neglecting radiative heat transfer also resulted in significantly higher temperatures. With radiation the maximum cell temperature was 1305 K. The maximum temperature was 37 K higher when radiation was neglected (Fig. 5). An overall stack temperature variation of 127 K was observed for the case with radiation and a 165 K variation was observed with radiation neglected.

The open circuit (or Nernst) voltage and the Ohmic losses are functions of the temperature. Therefore, variations in cell voltage are observed when there are temperature variations. When considering heat transfer only in a purely convective form, even under uniform flow conditions, noticeable variations in cell performance are observed. For the non-radiative case (purely convective heat transfer) a variation of 0.3% was obtained (Fig. 6). When radiative heat transfer was included the same trend in cell voltage variation occurred but with a variation $<0.2\%$. Variation in stack voltage with and without radiation was $<0.1\%$ for average current density of 3333 A/m^2. As shown later, these variations deteriorate significantly as flow distribution becomes non-uniform.

In summary, the influence of radiation is significant in estimating cell operating temperature. Neglecting radiation hinders heat transfer from the cell resulting in much higher stack temperatures and temperature gradients. For the case with an average current density of 3333 A/m^2 with uniform flow distribution, neglecting radiation did not yield significant cell voltage variations. However, results obtained with 6667 A/m^2 showed a much more significant cell voltage variation of 3.6% when radiation was neglected, while with radiation the variation was $<1.0\%$.

4.2. Effect of flow distribution—electrolyte supported cell

Larger variations in cell voltage were observed while performing a parametric study on the impact of flow distribution. It was shown that the greatest voltage variation occurred when 20% of the fuel flow in the bottom cell (cell 0) was directed to the neighboring cell (cell 1) this

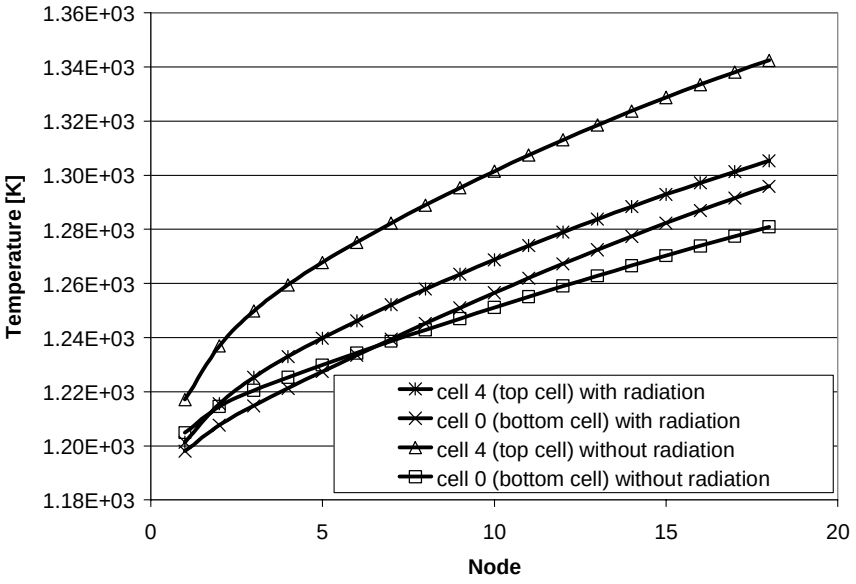

Fig. 5. PEN temperature comparison at average current density = 3333 A/m^2 with and without radiation.

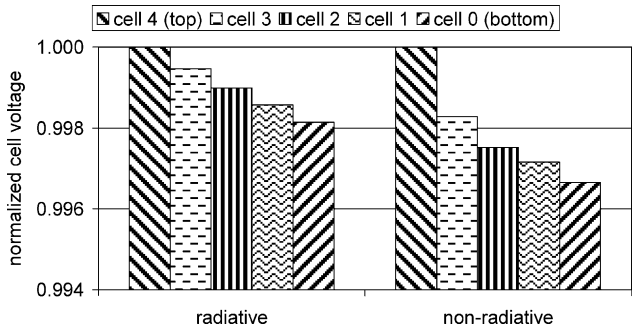

Fig. 6. Variation in cell voltage for uniform flow distribution at average current density = 3333 A/m^2 with and without radiative heat transfer. In each case, the cell voltage is normalized with the highest cell voltage.

corresponds to Case C in Table 3. As shown in Fig. 7, it was found that Case C resulted in approximately 3.5% variation in cell voltage. Radiative heat transfer did not eliminate the voltage variation caused by this non-uniform distribution. This variation is linked to the mole fraction of H_2 in Nernst equation (Eq. (10)).

Significantly larger cell voltage variations (12.3% at 6667 A/m^2) are likely when current densities are increased. These load conditions, however, are not likely when using electrolyte supported cells due to the high internal heating. As before, the inclusion of the radiative heat transfer reduces cell-to-cell voltage variations under these conditions, but significant variations are still present due to non-uniform distribution of fuel and oxidizer flow within the stack.

Regarding stack voltage variation, Fig. 8 shows *V–I* curves calculated for the case of an electrolyte supported cell with high oxygen utilization ($\dot{m}_{air} = 1.09 \times 10^{-3}$ kg/s) when radiation was neglected. These results indicate that the model was capable of capturing the typical polarization curve for a SOFC. The five-cell stack model captures the region of the polarization curve where the Ohmic loss dominates over the activation and concentration losses. Fig. 8

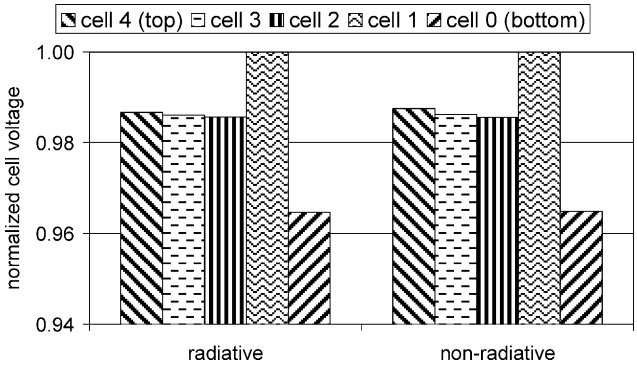

Fig. 7. Variation in cell voltage for non-uniform flow distribution (Case C) at average current density = 3333 A/m^2 with and without radiative heat transfer. In each case, the voltage is normalized with the highest voltage.

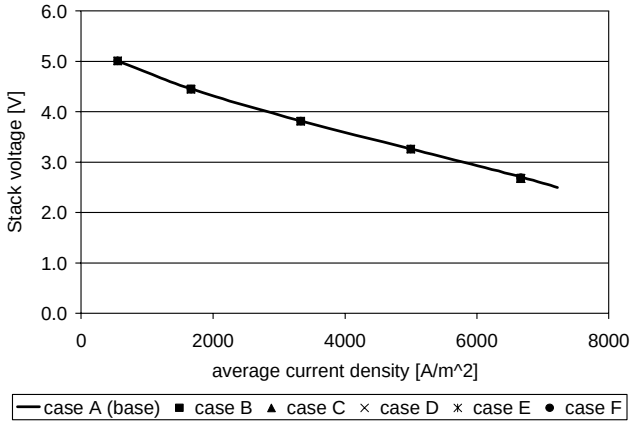

Fig. 8. Polarization curves for electrolyte supported five-cell stack.

also contains the stack *V–I* values for each of the six flow cases (Table 3). The stack voltage data points from the non-uniform cases coincide very closely with the data points from the uniform case. Thus while there exists performance variations within the stack (as discussed below), the overall stack *V–I* performance curve changes very little with flow distribution.

Therefore, it may be concluded that non-uniformity in flow distribution does not have a significant impact on the total stack voltage. While the highest stack voltage was obtained from a uniform flow distribution, for each case with non-uniform flow distribution the stack voltage differed by no more than 1.0% from the uniform case. Of greater interest, however, is the variation in cell voltage from cell-to-cell. This makes clear the need to monitor cell voltages in order to accurately assess the conditions inside a stack as they relate to flow upset conditions. In other words, mal functioning of a stack can not be detected by only monitoring the total stack voltage.

4.3. Impact of oxygen utilization—electrolyte supported cell

Changing the air mass flow rate resulted in different cell voltages. Such results are presented in Fig. 9, where for different current loadings the percent change in cell voltage (normalized by the highest cell voltage) is shown due to change in air flow rate from $\dot{m}_{air} = 5.45 \times 10^{-3}$ to $\dot{m}_{air} = 1.09 \times 10^{-3}$ kg/s. There is a pronounced change at higher current densities. For the case with average current density of 3333 A/m^2, the difference in cell voltage was <1%.

Thus it can be said that the oxygen utilization can have a large influence on the voltage variation for cases with high utilization. Different overall flow rates may result in different temperature distributions hence directly affecting the cell voltage distribution.

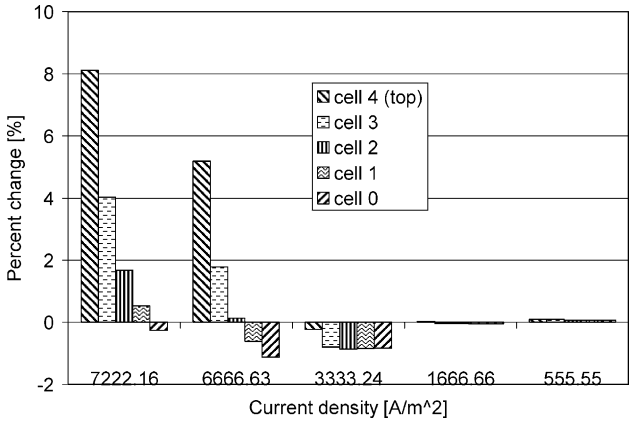

Fig. 9. Percent change in cell voltage due to change in air flow rate (oxygen utilization) for uniform flow distribution neglecting radiation.

4.4. Effect of radiation—anode supported cell

The operating temperature of the cells in the stack was greatly influenced by Ohmic heating caused by the resistance of the solid parts of the fuel cell. Changing the cell geometry from electrolyte to anode supported cell resulted in a change in resistance and thus less Ohmic heating. The anode supported geometry had an anode electrode thickness of 1.0×10^{-3} m supporting an electrolyte and cathode electrode of 1.0×10^{-5} and 2.5×10^{-5} m, respectively.

Fig. 10 shows the PEN temperatures for the top and bottom cells for the uniform flow distribution case with and without radiation. Similar to the electrolyte supported case (Fig. 5) neglecting radiation resulted in higher temperatures and large thermal gradients. The maximum temperature was 1462 K with radiation. Neglecting radiation resulted in temperatures as high as 1567 K. It is also noteworthy to observe

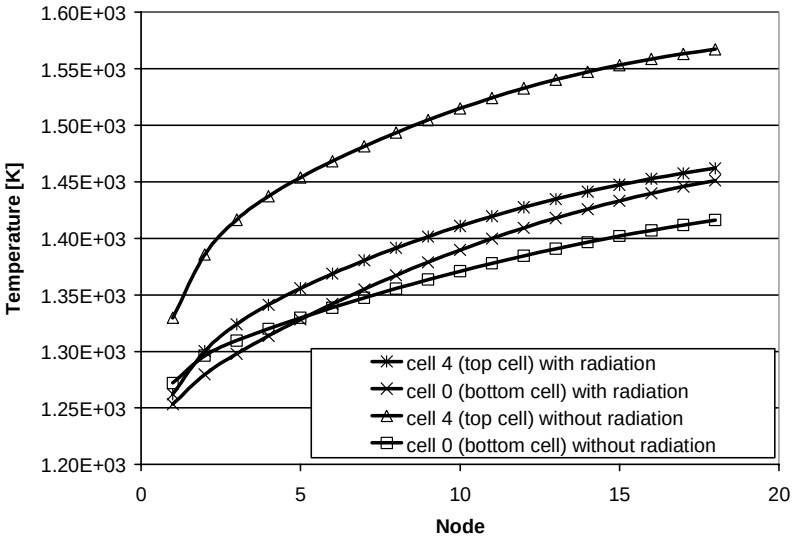

Fig. 10. PEN temperature comparison with and without radiation for anode supported geometry (with average current density = 6667 A/m^2).

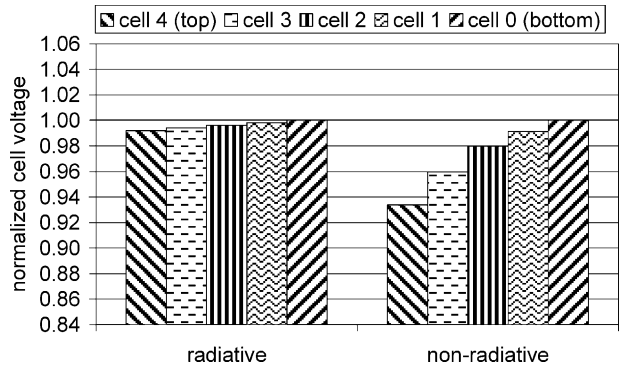

Fig. 11. Variation in cell voltage for uniform flow distribution with and without radiative heat transfer. In each case, the cell voltage is normalized with the highest cell voltage (with average current density = 6667 A/m^2).

that the overall thermal gradients in the axial direction are reduced by the effect of radiation.

The cell voltage variation is shown in Fig. 11 for the case with and without radiation. It can be seen that neglecting radiation resulted in approximately 7% variation in cell voltage. Inclusion of radiation reduced the variation to <1%.

Comparison of the anode and electrolyte supported geometry results, with radiation included, show that although the anode supported had less Ohmic heating the differences between the two types of cells are mostly negligible. The maximum temperature was approximately 9 K higher for the electrolyte supported case with the same operating conditions. Both geometries showed cell voltage variations of <1%. The influence of cell geometry was more significant when radiation was neglected. Without radiative effects the electrolyte supported case operating at an average current density of 6667 A/m^2 had an 3.6% variation in cell voltage while the anode supported case had a 6.6% voltage variation. These observations show that the cell-to-cell voltage variations are the result of a nonlinear coupling of flow distribution and cell geometry as well as temperature distribution.

5. Conclusions

The results of this study indicate that the variations in voltage among cells in a stack can be influenced by maldistribution of fuel and oxidizer flows. Cell-to-cell voltage variations occur partially due to the temperature non-uniformities within a stack of cells which results from naturally occurring asymmetry in planar stack design. The temperature gradient results in convective and radiative heat transfer among solid–gas and solid–solid components within the stack which helps to mitigate the temperature non-uniformities. When only convection/conduction heat transfer is considered large variations in cell performance was observed. The inclusion of radiative heat transfer in the mathematical model improved the uniformity of the temperature distribution within the stack thus leading to more uniform cell voltages. For the case of uniform flow distribution with radiation heat transfer, the cell-to-cell voltage variation was found to be <0.2%. This is smaller than the 0.3% variation obtained when considering only conduction/convection heat transfer. If the current demand is as high as 6667 A/m^2 there could be 3.6% variation in cell voltage. Redistribution of the fuel mass flow rate by c.a. 20% resulted in about 3.5% variation in cell voltage. Other case studies showed that at higher current densities variations in temperature and voltage can become more significant. Voltage variations of up to 12.3% were observed at 6667 A/m^2. The heat transfer model of this study is strictly applicable to “sandwich”-type fuel cells with a single fuel and oxidizer channel. This analysis can be extended to more complex multi-channel cells by expanding the heat transfer model in the separator regions and accounting for the geometric ratio of channel to separator-plate thickness. The present radiation model is quite simple in that it accounts only for first order effects. These trends need to be verified in a future work with more refined radiation models.

Acknowledgements

This study was funded by Department of Energy, National Energy Technology Laboratory, Morgantown, WV under Contract No.: Sub # 735934-30003-00, Task order: 735930-60008.

References

[1] M. Wójtowicz, S. Katianeni, R. Privette, The 2001 Symposium on Recent Advances in Fuel Cells, Fuel 81 (2002) 2147–2149.
[2] J. Billingham, A.C. King, R.C. Copcutt, K. Kendall, Analysis of a model for a loaded, planar, solid oxide fuel cell, Siam. J. Appl. Math. 60 (2) (2000) 574–601.
[3] A. Gubner, D. Froning, B. Haart, D. Stolten, Complete modeling of kW-range SOFC stacks, ECS Proc. 17 (2003) 1436–1441.
[4] G. Maggio, V. Recupero, C. Mantegazza, Modelling of temperature distribution in a solid polymer electrolyte fuel cell stack, J. Power Sources 62 (1996) 167–174.
[5] P. Costamagna, E. Arato, E. Achenbach, U. Reus, Fluid dynamic study of fuel cell devices: simulation and experimental validation, J. Power Sources 52 (1994) 243–249.
[6] H. Hirata, M. Hori, Gas-flow uniformity and cell performance in a molten carbonate fuel cell stack, J. Power Sources 63 (1996) 115–120.
[7] P. Costamagna, K. Honegger, Modeling of solid oxide heat exchanger integrated stacks and simulation at high fuel utilization, J. Electrochem. Soc. 145 (11) (1998) 3995–4007.
[8] E. Achenbach, Three-dimensional and time-dependent simulation of a planar solid oxide fuel cell stack, J. Power Sources 49 (1994) 333–348.
[9] Z. Ma, A combined differential and integral model for high temperature fuel cells, Ph.D. Thesis, Georgia Institute of Technology, Georgia, 2000.
[10] J. Yuan, M. Rokni, B. Sundén, Three-dimensional computational analysis of gas and heat transport phenomena in ducts relevant for anode supported solid oxide fuel cells, Int. J. Heat Mass Transfer 46 (2003) 809–821.
[11] D. Krotz, Almost there: a commercially viable fuel cell, 2003, http://enews.lbl.gov/Science-Articles/Archive/MSD-fuel-cells.html.

[12] P. Aguiar, D. Chadwick, L. Kershenbaum, Modelling of an indirect internal reforming solid oxide fuel cell, Chem. Eng. Sci. 57 (2002) 1665–1677.
[13] H. Yakabe, M. Hishinuma, M. Uratani, Y. Matsuzaki, I. Yasuda, Evaluation and modeling of performance of anode-supported solid oxide fuel cell, J. Power Sources 86 (2000) 423–431.
[14] A. Virkar, J. Chen, C. Tanner, J. Kim, The role of electrode microstructure on activation and concentration polarizations in solid oxide fuel cells, Solid State Ion. 131 (2000) 189–198.
[15] A.C. Burt, I.B. Celik, R.S. Gemmen, A.V. Smirnov, Influence of radiative heat transfer on variation of cell voltage within a stack, in: Proceedings of the First International Conference on Fuel Cell Science, Engineering and Technology, Rochester, New York, 21–23 April 2003.
[16] A.C. Burt, I.B. Celik, R.S. Gemmen, A.V. Smirnov, Cell-to-cell performance variations within a stack, in: Proceedings of Eighth International Symposium on SOFC (SOFC-VIII), Paris, France, 27 April–2 May, 2003.
[17] R. Gemmen, E. Liese, J. Rivera, F. Jabbari, J. Brouwer, Development of dynamic modeling tools for solid oxide and molten carbonate hybrid fuel cell gas turbine systems, in: Proceedings of the International Gas Turbine Institute Meeting of the American Society of Mechanical Engineers, 8–12 May 2000.
[18] A.F. Mills, Basic Heat and Mass Transfer, Irwin, Chicago, 1995.
[19] R. Siegel, J. Howell, Thermal Radiation Heat Transfer, McGraw-Hill, New York, 1972.
[20] W.Z. Zhu, S.C. Deevi, Opportunity of metallic interconnects for solid oxide fuel cells: a study on contact resistance, Mater. Res. Bull. 38 (2003) 957–972.